Neurotherapeutics 21 (2024) e00295

Contents lists available at ScienceDirect

Neurotherapeutics

journal homepage: www.sciencedirect.com/journal/neurotherapeutics

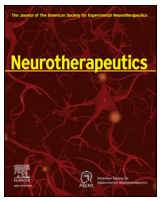

Original Article

Thalamo-cortical evoked potentials during stimulation of the dentato-rubro-thalamic tract demonstrate synaptic filtering

Christopher R. Conner [a,*], Kiefer J. Forseth [c], Andres M. Lozano [b], Robert Ritter III [d], Albert J. Fenoy [e,*]

[a] Division of Neurosurgery, Department of Surgery, University of Connecticut, Hartford, CT, USA
[b] Division of Neurosurgery, Department of Surgery, University of Toronto, Toronto, Ontario, Canada
[c] Division of Neurosurgery, University of California San Diego, San Diego, CA, USA
[d] Department of Neurosurgery, University of Texas Health Sciences Center at Houston, Houston, TX, USA
[e] Department of Neurosurgery, Donald and Barbara Zucker School of Medicine at Hofstra/Northwell, Feinstein Institutes for Medical Research, Manhasset, NY, USA

ARTICLE INFO

Keywords:
Deep brain stimulation
Essential tremor
Evoked potential
Phase-amplitude coupling

ABSTRACT

Essential tremor DBS targeting the ventral intermediate nucleus (Vim) of the thalamus and its input, the dentato-rubro-thalamic tract (DRTt), has proven to be an effective treatment strategy. We examined thalamo-cortical evoked potentials (TCEPs) and cortical dynamics during stimulation of the DRTt. We recorded TCEPs in primary motor cortex during clinical and supra-clinical stimulation of the DRTt in ten essential tremor patients. Stimulation was varied over pulse amplitude (2–10 mA) and pulse width (30–250 μs) to allow for strength-duration testing. Testing at clinical levels (3 mA, 60 μs) for stimulation frequencies of 1–160 Hz was performed and phase amplitude coupling (PAC) of beta phase and gamma power was calculated. Primary motor cortex TCEPs displayed two responses: early and all-or-none (<20 ms) or delayed and charge-dependent (>50 ms). Strength-duration curve approximation indicates that the chronaxie of the neural elements related to the TCEPs is <200 μs. At the range of clinical stimulation (amplitude 2–5 mA, pulse width 30–60 μs), TCEPs were not noted over primary motor cortex. Decreased pathophysiological phase-amplitude coupling was seen above 70 Hz stimulation without changes in power spectra and below the threshold of TCEPs. Our findings demonstrate that DRTt stimulation within normal clinical bounds does not excite fibers directly connected with primary motor cortex but that supra-clinical stimulation can excite a direct axonal tract. Both clinical efficacy and phase-amplitude coupling were frequency-dependent, favoring a synaptic filtering model as a possible mechanism of action.

Introduction

Deep brain stimulation (DBS) for tremor and Parkinson's disease was demonstrated by Brice et al., in 1980 and approved by the FDA 17 years later [1]. Despite the growing use of this treatment, the physiologic mechanism of DBS is an open area of investigation [2]. Classical theory is that neuronal somata are inhibited [2,3] while axons are excited [4], and that DBS functions via a lesion-type effect. However, recent work has given rise to several new models. While axons can transmit at clinical stimulation frequencies above 100 Hz, it is unlikely that synapses can as this will deplete neurotransmitters and low pass filter signals in a process called synaptic filtering [5,6]. Stimulation could also prevent the transmission of physiologic signals by overloading axonal transmission via blockade [7].

To test the interaction of axonal blockade and synaptic filtering, we targeted axons within a white matter fiber pathway – the dentato-rubro-thalamic tract (DRTt). The DRTt connects the dentate nucleus of the cerebellum with the ventral intermediate nucleus of the thalamus (Vim) via the red nucleus [8–11] and has been a successful DBS target for the treatment of essential tremor. DBS was performed at supra-clinical levels using a wide range of stimulation pulse shapes (amplitude and width) and across a broad frequency range in 10 subjects. We first used thalamo-cortical evoked potentials (TCEPs) measured in primary motor cortex (M1) to analyze which neural elements were activated during low-frequency

* Corresponding authors.
E-mail addresses: chconner@uchc.edu (C.R. Conner), afenoy@northwell.edu (A.J. Fenoy).

https://doi.org/10.1016/j.neurot.2023.10.005
Received 10 October 2023; Accepted 10 October 2023

stimulation (1 Hz). By varying the stimulation amplitude and pulse duration over an extensive range (1.25–10 mA and 30-250mcS, respectively), we estimated the strength-duration curve [12] of the DRTt and examined how axonal blockade could contribute to DBS of the DRTt. Next, the frequency was modulated (1–160 Hz) at a stimulation level below the threshold of TCEPs. This paradigm tested if a frequency-dependent process, such as synaptic filtering, can result in measurable electrophysiology response in M1.

Methods

Subjects

Patients with a history of disabling essential tremor (ET) were recruited after evaluation for deep brain stimulation (DBS) treatment. Patients were candidates for surgery given their disease length, severity, and quality of control on medications. Before surgery, patients were counseled on the risks and benefits of participating. They gave written consent to participate per NIH guidelines as monitored by the University of Texas, Houston (UTH) Institutional Review Board (IRB).

A total of 10 patients were enrolled in the study (Table 1). All patients had subdural electrodes (SDEs) implanted on the side contralateral to their more severe symptoms. Three patients were more symptomatic on the left side and thus had right-sided SDEs placed (pts. 1, 7, and 8). All other patients had more severe right-sided symptoms and were implanted on the left (only pt. no 1 self-described as “left-handed,” others reported they were “right-handed”).

Imaging acquisition

Pre-operatively, MRI data were acquired on a 3T Hdxt Release 16.0 Twin speed MR imaging system (GE Healthcare, USA). A T2-weighted 3D isotropic sequence was acquired in the sagittal orientation (3000 ms TR, 66.9 ms TE, FOV 24 mm, 288 × 288 matrix, 190 slices, thickness 1.0 × 1.0 mm isotropic slices). The resulting data were reconstructed to 1.0 mm^3 isotropic voxels. For diffusion tensor imaging, we applied a spin-echo echo-planar imaging pulse sequence (17,000 ms TR, 86.3 ms TE, FOV 25 mm, 128 × 128 matrix; 66 slices, 2.0 mm slice thickness, 32 gradient directions, 1000 s/mm^2 b-value). The sequence resulted in 2.0 mm^3 isotropic reconstructed voxels acquired in the axial orientation.

Surgical procedure

Bilateral DBS electrodes (model 3387, four 1.5 mm contacts with 1.5 mm spacing, Medtronic, Inc.) were stereotactically implanted using the Leksell frame (Elekta, Sweden) following our established protocol [13]. Surgery was performed with the patient awake and predominantly under local anesthesia using mild sedation with propofol (Diprivan, AstraZeneca, London) during burr hole placement. Each patient's dentato-rubro-thalamic tract (DRTt) is individually mapped by deterministic fiber tracking from the diffusion tensor MRI. Using StealthViz software (Medtronic, Inc.), identification of the DRTt was performed by seeding the fiber tracking algorithm in the dentate nucleus. All fibers passing through the superior cerebellar peduncle and up to the contralateral hand primary motor cortex were included. A point within the resulting tract in the anterior commissure-posterior commissure plane was selected as the target for the first contact of the DBS lead.

Intra-operative DBS efficacy was tested under clinical range parameters (stimulation frequency 100–130 Hz, 2–5 V, pulse width 30–90 μs) during simple motor tasks. Tremor control was continuously monitored by the neurosurgical team and a neurologist specializing in movement disorders. After successful clinical trialing, the clinical external pulse generator was disconnected. Intraoperative control of tremor was seen during stimulation at 2–4 V, a pulse width 30–60 μs, and frequency of 120–160 Hz in all subjects.

Electrode localization and visualization

The T1 anatomical MRI for each subject was used to construct mesh models of the gray/white matter interface and pial surface using FreeSurfer v4.5 [14,15]. Following electrode implantation, a high-resolution contiguous thin-slice CT scan was acquired (0.5 mm in-plane resolution, 1 mm thick axial slices). This CT scan was co-registered to the pre-operative anatomical MR imaging using a rigid-body transformation algorithm implementing a mutual information cost function [16]. The centers of individual electrodes were localized using the post-operative CT and then transformed into the image space of the anatomical MRI. To visualize all these elements concurrently, we defined planes by the DBS lead, the M1 contacts, and the lateral axis; the pial mesh model was cut along this plane, and interior points were interpolated from the T1. The DRTt was then displayed as a volume in the same imaging space as the surface (threshold at >200 fibers).

Thalamo-cortical evoked potentials

Before DBS lead implantation, either an 8- or 12-contact SDE strip was passed posteriorly through the access burr hole. Position over M1 is confirmed using intra-operative CT merged with the pre-operative anatomical MRI. A separate 4-contact strip was placed in the sub-galeal space and served as ground and reference for recordings. The electrodes were connected to a NeuroFax (Nihon Kohden) recording system,

Table 1
Patient demographics.

Pt. No.	Age	Sex	Hand	SDEs	TCEPs	CD	PAC	DBS settings
1	63	F	Left	Right	Y	N	N	1.5 V, 60 μs, 130 Hz
2	64	F	Right	Left	Y	N	N	1.5 V, 60 μs, 170 Hz
3	67	M	Right	Left	Y	Y	N	2.5 V, 60 μs, 130 Hz
4	45	F	Right	Left	Y	Y	N	3.6 V, 60 μs, 170 Hz
5	86	F	Right	Left	Y	Y	Y	5.5 V, 140 μs, 140 Hz
6	80	M	Right	Left	Y	Y	Y	2.5 V, 90 μs, 160 Hz
7	68	M	Right	Right	Y	Y*	Y	1.8 V, 60 μs, 140 Hz
8	68	M	Right	Right	Y	Y*	Y	3.2 V, 70 μs, 180 Hz
9	63	M	Right	Left	Y	N	Y	5 V, 80 μs, 165 Hz
10	61	F	Right	Left	Y	N	Y	3.2 V, 90 μs, 165 Hz

Three different experimental paradigms were used: thalamo-cortical evoked potentials (TCEPs), charge density (CD) for strength-duration estimation, and phase-amplitude coupling. In two patients, additional CD testing was performed at lower amplitude and shorter duration than in other patients (pts. 7 and 8, labeled “Y*”). In the final two patients, only PAC was carried out due to experimental time constraints. Pt 8 did not have DTI as they had hardware that was not 3T MRI compatible. Mean DBS stimulation voltage was 3.0 V (1.34 V sd), and with a total system resistance of 1000–1200 Ohms, this is approximately 3 mA as used in our stimulation protocol. All patients were programmed in a configuration of 1−/2+ for clinical optimization.

and electrocorticography (ECoG) was collected at 1 kHz. An ECoG recording was collected for 2–5min immediately after SDE placement while the patient was at rest. This recording serves as a baseline since DBS lead implantation in the DRTt can result in a transient "lesion effect" and improvement of symptoms [8]. If a lesion effect occurs, there is the possibility that cortical activity will be altered by DBS lead placement and alter baseline ECoG phenomena. The surgery then proceeds with DBS implantation as described above.

Using the Medtronic twist-lock screening cable (model 3550-03) and a custom adapter, the DBS lead was connected to an external pulse generator (S88X; Grass Instruments, Quincy, MA) and photoelectric constant-current stimulus isolation unit (SIU-BI, Grass Instruments). Post-modification impendence of the cable and adapter was compared with Medtronic guidelines and was grossly consistent (<5 Ohm before and after modification). Before stimulation for each patient, the impedance of the whole system was tested and verified to be within manufacturer specification (typically 1000–1200 Ohm).

DBS electrode leads were first stimulated during ECoG recording in contact pairs with bipolar, balanced square-wave pulses (2.5 and 5 mA, 250 μs in each phase, at 1 Hz for 30 s). DBS contacts are numbered 0, 1, 2, 3, with 0 as the distal contact and 3 as the proximal. Pairwise stimulation was performed with 0−/1+, 1−/2+, and 2−/3+ (− for the cathode and + for the anode). DRTt targeting with our protocol typically results in 1−/2+ as the contact pair with the greatest clinical effect, and this pair was used for experiment stimulation.

ECoG data collected during stimulation are exported to Matlab for processing (bandwidth 0.2–300 Hz), and epochs were time-locked at the beginning of each stimulus [17]. Positive and negative deflections in the averaged TCEP were identified using the Matlab (Mathworks, ver 2021b) function *findpeaks*. Following the stimulus artifact, the first negative deflection was defined as an N1 response [17,18]; the following positive deflection was labeled P1. The peak amplitude and prominence (a modified area under the peak) for each deflection was calculated by *findpeaks*.

Strength-duration testing

In 6 of the 10 patients, additional TCEPs were collected at a wider range of pulse widths and stimulus amplitudes. This paradigm, referred to as charge density testing, was performed using DBS contacts 1−/2+. Pulse width ranged from 30 to 250 μs, pulse amplitude from 1.25 to 10 mA, and charge density from 2.5 to 20 μC/cm^2 (Table 2). Charge density (in μC/cm^2) can be calculated from pulse amplitude, I in mA; pulse width, PW in μs; and contact area, A in cm^2.

$$CD = \frac{(I \times PW)}{A}$$

For a contact area of 0.06 cm^2, maximal charge density was kept under 30 μC/cm^2 to prevent tissue damage [19–21]. The pairs of widths and amplitudes were chosen to have set charge density levels to allow for comparisons of different parameters in multivariate regression. Stimulation was performed at 1 Hz for at least 25 sweeps.

Table 2
Charge density stimulation parameters.

Pulse width (μs)	Pulse amplitude (mA)	Charge density (μC/cm^2)
30	5	2.5
30	10	5
60	2.5	2.5
60	5	5
60	10	10
120	2.5	5
120	5	10
120	10	20
250	1.25	5
250	2.5	10
250	5	20

Stimulation was varied in pulse width and amplitude, and multiple combinations of both were chosen to test set charge density levels. Given that the system has a total resistance of approximately 1 kOhm, a 1 mA pulse has a potential of 1 V.

Peak amplitude and prominence for each stimulation parameter were calculated for all M1 electrodes across subjects. Two generalized linear models (GLM) were fit using peak amplitude and peak prominence as dependent variables. Regressors included pulse width, pulse amplitude, and CD. Patient and electrode were included as fixed effects. The equation for the first GLM was:

$$peak\ amplitude \sim \beta_0 + \beta_1 \times PW + \beta_2 \times I + \beta_3 \times CD + \varepsilon_{electrode} + \varepsilon_{patient}$$

And for the second GLM:

$$peak\ prominence \sim \beta_0 + \beta_1 \times PW + \beta_2 \times I + \beta_3 \times CD + \varepsilon_{electrode} + \varepsilon_{patient}$$

The fit was assessed with the correlation coefficient. Model reduction was performed using stepwise Aikake information criteria (AIC) with the *stepAIC* function in R (ver 3.6.2, CRAN and R Foundation for Statistical Computing). Overfitting was initially assessed with Cook's and normal Q-Q plots.

Phase amplitude coupling

Using clinical stimulation parameters (pulse width 30 μs, amplitude 3 mA), 10 s duration trains were applied at increasing frequencies. Stimulation was performed at 1, 2, and 5 Hz, then from 10 to 160 Hz in 10 Hz increments from a total of 6 patients (Table 1). Each 10s epoch was assessed for changes in spectral power in both the beta (13–30 Hz) and gamma (>30 Hz) frequency ranges using power spectral density (Welch's method, Hanning window of 256 ms, 50 % overlap).

The phase-amplitude coupling (PAC) was calculated for each epoch using the co-modulation index method [22,23]. The frequency ranges were 12–20 Hz for beta and 30–200 Hz for gamma. In two patients with minimal 60 Hz line noise, the gamma range was set to 80–200 Hz (pt. no. 6 and 8). PAC was compared with baseline recording prior to insertion of DBS lead. The PAC for beta-gamma coupling was calculated for all other electrodes outside M1. A *t*-test was computed for each stimulation frequency (1–160 Hz) of the M1 electrodes against non-M1 electrodes. The t-values for the M1 electrodes were then averaged across subjects (Fig. 1).

Results

Thalamo-cortical evoked potentials

Stimulation of the DRTt at 1 Hz resulted in reproducible TCEPs within M1. Three phases of TCEPs (Fig. 2) were noted: early N1 (<20 ms after stimulation), subsequent P1 (30–70 ms), and late N2 (70–150 ms). Amplitude and prominence of each TCEP increased with both stimulation amplitude and pulse width. However, stimulation within the clinical range of parameters (2–5 mA, 30–60 μs) did not reliably generate an N1 TCEP but was able to elicit a P1 in some patients. After approximately 150 ms, recordings returned to baseline activity for all stimulus parameters.

Multivariate regression was fitted with pulse amplitude, pulse width, and CD as regressors on peak amplitude and prominence for the N1, P1, and N2 potentials to determine the effect of stimulation parameters on TCEP components. The N1 potential varied minimally over the range of stimulation parameters (Fig. 2) but only above a total current density of 5 μC/cm^2. However, for M1, the P1 potential morphology was significantly correlated with pulse amplitude ($t = 3.88$, $p < 0.001$, $df = 184$, $r^2 = 0.87$) and CD ($t = 5.11$, $p < 10^{-6}$), while N2 only correlated with CD ($t = 4.38$, $p < 10^{-4}$, $r^2 = 0.66$). Pearson's correlation between N1 and the P1 and N2 TCEPs was 0.66 for both ($t = 12.5$ and 12.6, respectively, with $df = 206$, $p < 0.001$).

Strength-duration analysis requires stimulation at a variety of pulse widths and amplitudes as was performed here [12]. A pulse width of 250 μs is significantly longer than is typical for clinical DBS but only gives an estimation of the rheobase of the neural elements being excited. At this

pulse width, the minimum current required for an N1 potential is approximately 1–1.25 mA. From this estimate, the chronaxie can be seen on the current density graph (Fig. 2) and would be approximately 100–120 μs. Stimulation at 120 μs and 2.5 mA does produce an N1 TCEP with amplitude, prominence, and morphology similar to other combinations with a current density of 5 μC/cm^2.

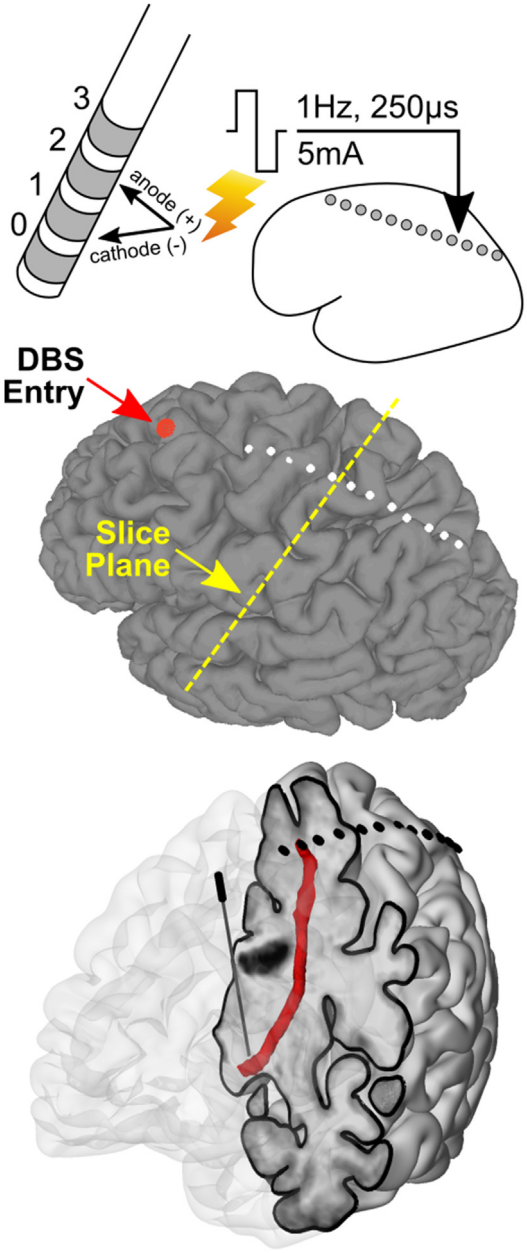

Fig. 1. Experimental design using DBS lead stimulation and subdural electrodes for recordings. DBS leads are inserted into the DRTt just inferior to the Vim nucleus of the thalamus. Each lead contains four contacts, which can be stimulated in pairs using balanced square wave pulses of varying width and amplitude, and at frequencies over 150 Hz. Subdural electrodes are then visualized on a pial surface reconstructed from the T1 MRI; the DBS lead's entry point is displayed as a red sphere. A cutaway model of the brain shows the position of the DBS lead within the brain and fibers leaving the M1 SDEs passing by the DBS lead.

Phase-amplitude coupling

Beta (12–20 Hz) phase and gamma (30–200 Hz) amplitude coupling (PAC) was estimated [24] over a frequency range (1, 2, 5, then 10–160 Hz in 10 Hz increments, pulse width 30 μs, amplitude 3 mA) and compared with baseline. PAC over M1 was elevated compared with recordings outside M1 (Fig. 3) as seen in the average t-value of M1 SDEs. However, PAC decreased linearly as a function of stimulation frequency and the PAC of M1 SDEs was below baseline around 70 Hz. Decreasing PAC continued until it was not significantly different at around 130 Hz. Averaged frequency-by-frequency plots of M1 PAC were computed for stimulation frequencies of 40–150 Hz and confirm broadband PAC changes over this stimulation range (Fig. 4). Finally, averaged power spectral density (PSD) was computed for stimulation at 60–90 Hz confirmed that power before, during, and after stimulation was not significantly different other than stimulation artifact (Fig. 5).

Discussion

In this study, we have performed stimulation experiments and collected cortical TCEPs on a previously untested target – the dentato-rubro-thalamic tract. Our goal was to assess both evoked potentials and network effects over a range of stimulation parameters and begin examining possible DBS mechanisms for the DRTt. We found that within the stimulation range sufficient for clinical efficacy, no early (<10 ms) M1 TCEP was measured, indicating that the DRTt does not directly connect to primary motor cortex. Using stimulation over a range of frequencies, we found that pathological PAC between beta and gamma frequencies had a linear decrease starting at around 70 Hz. At the same time, there was no underlying change in power of either frequency band. This finding fits well with the long-term stimulation settings used for clinical effect in this patient group [25,26].

Strength-duration testing

While stimulation on the order of 250 μs will only give a rough estimate of rheobase [27,28], we measured the strength-duration curve at four different pulse widths (30, 60, 120, 250 μs). We found that the threshold current density (total charge) for TCEPs was ~5 μC/cm^2 and did not increase with pulse width as might be expected [29]. The TCEP morphologies were also similar for each level of current density (5, 10, 15, and 20 μC/cm^2), and the amplitudes of N1/P1/N2 were correlated with each other. These findings indicate that the strength-duration curve has a shallow or flat slope for this range of stimulation parameters. It is difficult to precisely extract the chronaxie from such data [30], but they indicate that it would be <200 μs and consistent with axonal activation [12]. Increasing TCEP amplitude at higher current injections would then be secondary to greater recruitment of fibers [31,32].

The DRTt and primary motor connectivity

Large, myelinated axons have lower activation thresholds than soma or dendrites [27,31], yet we found that stimulation at 30–60 μs and <5 mA was insufficient to generate early TCEPs (<20 ms, N1) in primary motor cortex. Without an early TCEP, there is no indication that DRTt stimulation in the range of clinical stimulation activates axons that directly connect to M1. However, DBS at this location may result in an axonal blockade of information flow into Vim from the red and dentate nuclei [7]. One of the primary models for ET is the effect of cerebellar bursting on Vim [4]. Any disruption of pathological information flow into the Vim could then have a downstream

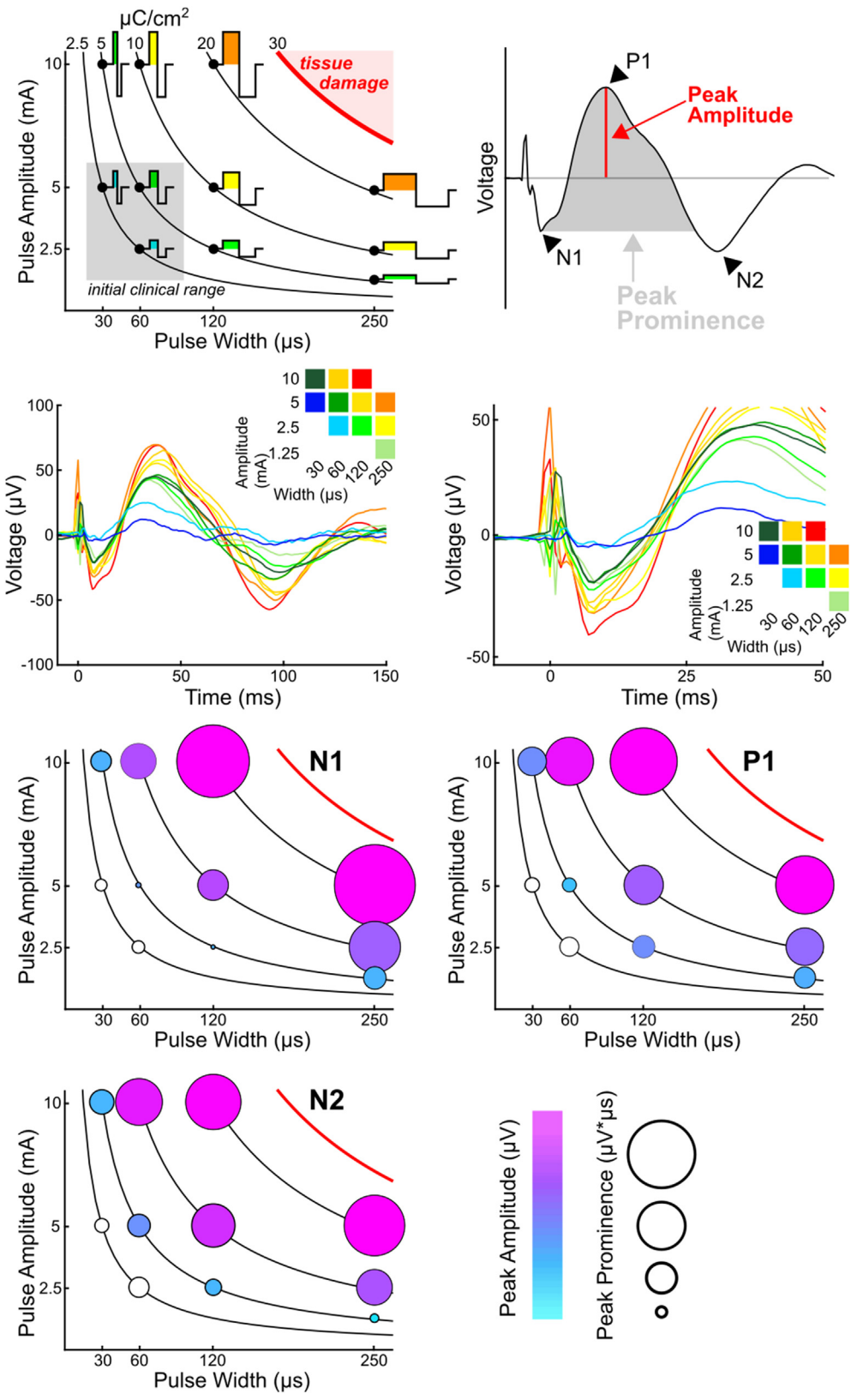

Fig. 2. Thalamo-cortical evoked potentials (TCEPs) are dependent on the charge density of stimulation. Pulse widths and amplitude were varied from clinical to supra-clinical (30–250 μs and 1.25–10 mA, all stimulation at 1 Hz) at a variety of amplitude-width pairs while controlling for charge density (2.5, 5, 10, and 20 μC/cm^2). These parameters allowed for direct evaluation of the contribution of amplitude, pulse width, and charge density to TCEP morphology. Peaks were quantified by amplitude or prominence (or area-under-the-curve/AUC). The P1 and N2 TCEPs (first positive and second negative deflections) showed the greatest levels of variability. Scale bars for charge density graphs - N1: 20–60 μV and 50–100 μV* μs, P1: 30–80 μV and 60–135 μV* μs, and N2: 40–65 μV and 70–125 μV* μs.

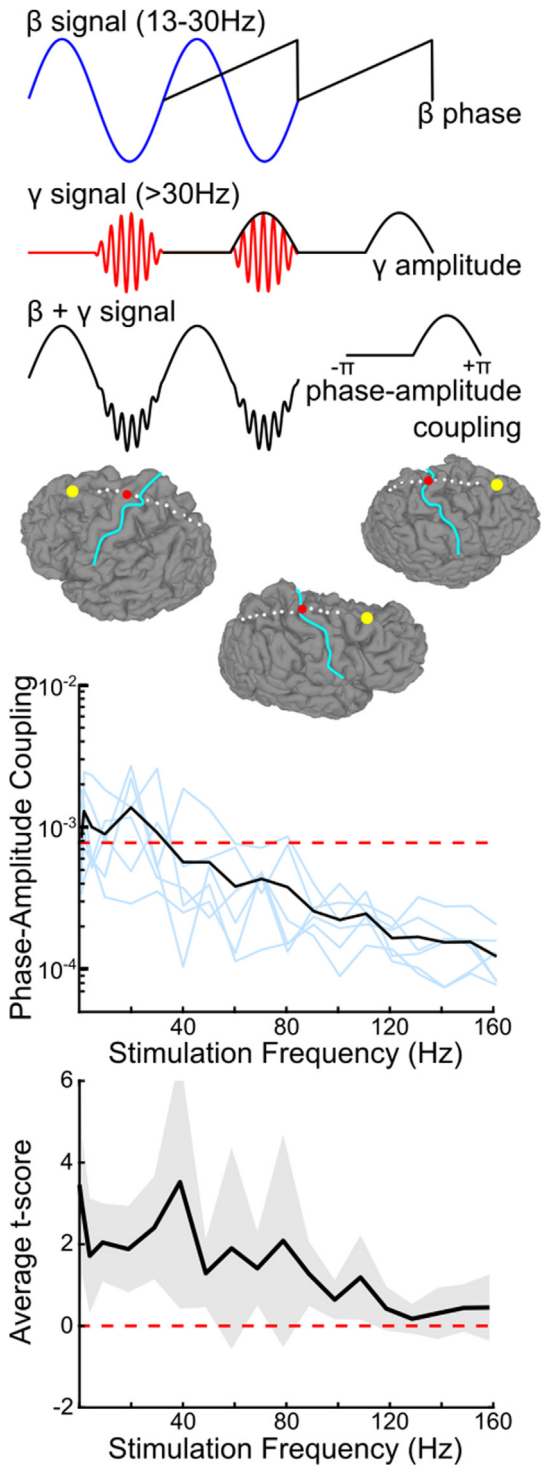

Fig. 3. Phase amplitude coupling (PAC) decreases with increasing stimulation frequency. PAC was assessed as the relationship between beta (13–30 Hz) phase and gamma (30–200 Hz) amplitude. SDEs from six patients over M1 were included. PAC was high at baseline and during low frequency (<70 Hz) stimulation, but above 70 Hz resulted in a linear decrease in PAC. A baseline PAC from before DBS lead insertion is included for reference (dotted red line). The PAC for M1 SDEs was then compared with all non-M1 SDEs to estimate the significance (shown with ± 2 s.e.m., red dotted line denotes a t = 0).

effect on primary motor cortex as measured with PAC or observed clinically. The N1 TCEPs noted at higher charge density (above the clinical range) are thought to be mediated by volume conduction [31].

Phase amplitude coupling and synaptic filtering

The clinical effect of DBS on tremor has been previously shown to increase linearly with stimulation frequency. In prior reports on STN, tremor control begins around 70 Hz and increases until leveling off at 130Hz [33]. Our results demonstrate that, like STN, the key stimulation parameter for the efficacy of DRTt DBS is frequency [34]. The linear trend between 70 and 130 Hz was seen in the decrease of pathological PAC seen in M1, matching with the clinical parameters for the patients and in prior work [4,35]. Notably, increased gamma-beta PAC has been shown before in Parkinson's patients, and breaking this pattern was correlated with clinical response [25]. The results here are the first to demonstrate this relationship over a wide range of stimulation frequencies (1–160 Hz) and for the DRTt.

Resonance of evoked potentials

A stimulation frequency of 1 Hz allows for a sufficient interstimulus interval to observe long-latency EPs. With this approach, we resolved repeatable TCEPs at over 100 ms after stimulation. The P1 and N2 amplitudes were significantly correlated with the N1 TCEPs. This relationship is a product of their collective dependence on the stimulation parameters, but there is also the possibility of network reverberations or dampened resonance [36,37]. The morphology of the N1 is sharper in its rise and fall, whereas the P1 and N2 are stretched potentially by transmission along fiber pathways and pre-/post-synaptic processing. It is notable that even though clinical range stimulation does not elicit an N1 response, there were measurable P1 and N2 responses in some patients suggesting that network reverberation is present. However, an important component of resonance as a mechanism is a change in the fundament oscillating frequency in response to these EPs traveling through the network [36,38]. Changes in network oscillation (noted in beta or gamma power in M1, Fig. 5) were not observed at clinical stimulation parameters.

Limitations

Studies focused on DBS-induced cortical EPs are primarily based on intra-operative recordings where time is at a premium. Without indefinite duration experiments, the ability to perform rigorous strength-duration curve testing is limited compared to the laboratory setting [12]. This is compounded by an inability to perform real-time analysis to verify the repeatability of evoked potentials and determine if a given stimulus has reached threshold. The operating room can be electrically noisy with numerous sources of 60 Hz line interference and artifact sources that cannot be turned off (e.g., ventilators). Patients have variable anesthesia needs, which can lead to differences in pharmacology. All patients were sedated using dexmedetomidine during the opening portion of the procedure and this was stopped after drilling of the access burr holes. The recording system used here has a sampling frequency of 1 kHz, limiting the ability to resolve early evoked potentials [18,31,39,40]. This is compounded by the presence of stimulation artifact that obscured deflections with latency <3–5 ms. However, a translational research paradigm does allow for testing with a high number of subjects, greater distance between stimulation source and recording site than in non-human primates, and collection of clinical-grade imaging with a variety of modalities.

Overall, these results represent the first strength-duration style experiments performed on a white-matter target, the DRTt, and a study of frequency-specific cortical responses over a wide parameter space. We have demonstrated that the stimulation target is not a direct axonal fiber bundle from the DBS lead to primary motor cortex but rather Vim or its input. DBS efficacy here has a linear response to an increasing frequency as measured with PAC and mirrored in clinical settings. Ongoing work will focus on the effect of stimulation frequency on motor cortex dynamics to optimize DBS for essential tremor.

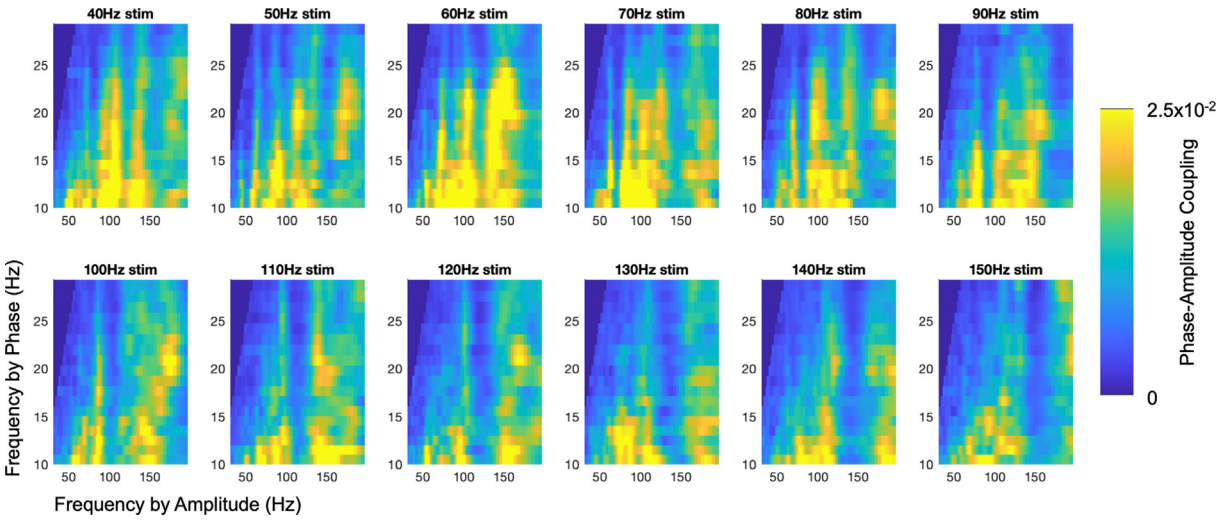

Fig. 4. Phase-amplitude coupling (PAC) by frequency. PAC plots (frequency by phase, frequency by amplitude) for different stimulation frequencies are shown for beta phase (10–30 Hz) and gamma amplitude (30–200 Hz). Results are averaged across the same electrodes used the PAC analysis (Fig. 4). There broadband decrease in PAC across beta-gamma coupling at stimulation above 70 Hz. PAC units are arbitrary.

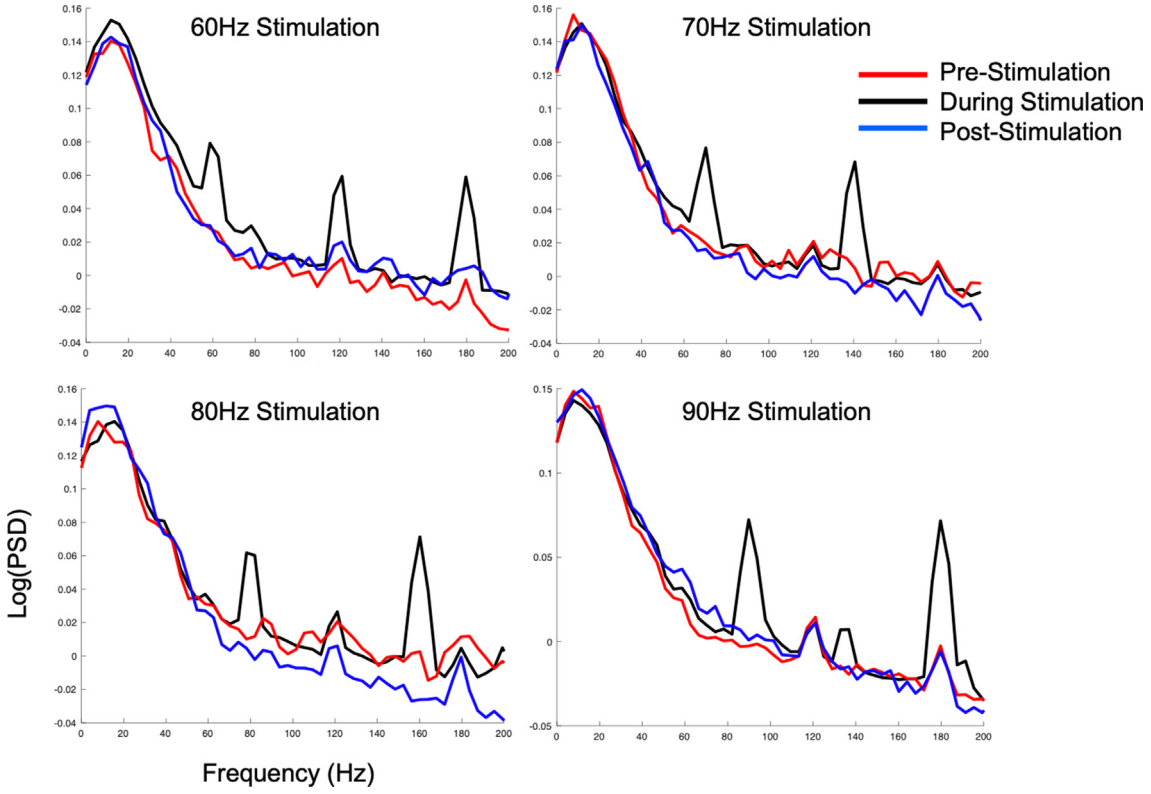

Fig. 5. Power spectral density (PSD) estimates around stimulation. PSD was calculated using Welch's method (Hanning window of 256 ms, 50 % overlap) for the 2 s before stimulation (red, Pre-Stimulation), the 10 s during stimulation (black), and the 2s after stimulation stopped (blue, Post-Stimulation). PSDs for stimulation at 60, 70, 80, and 90 Hz are shown. Results are averaged across the electrodes used from the PAC analysis (Fig. 4). Each demonstrates a low frequency peak within the beta range (10–30 Hz), and a power-law decrease in the gamma range. Stimulation artifacts are seen at the frequency of stimulation and harmonics above that. Overall, the log (PSD) is stable in both the gamma and beta ranges.

Declaration of competing interest

The authors declare that they have no known competing financial interests or personal relationships that could have appeared to influence the work reported in this paper.

Acknowledgments

All authors contributed to the final manuscript. CC data collection and mathematical analysis. CC and KF data processing. KF neuroimaging processing and visualization. AL results interpretation and data analysis.

AF clinical management and patient recruitment. We thank our patients for their participation. We also thank E Rupert and J Bielat for intra-operative assistance during surgery. This study was funded by the NIH (R01 NS113893 to AF) and a grant from the Society of Neurological Surgeons (to CC).

References

[1] Brice J, Mclellan L. Suppression of intention tremor by contingent deep-brain stimulation. Lancet 1980;315:1221–2.
[2] Perlmutter JS, Mink JW. Deep brain stimulation. Annu Rev Neurosci 2006;29:229–57.
[3] Ashkan K, Rogers P, Bergman H, Ughratdar I. Insights into the mechanisms of deep brain stimulation. Nat Rev Neurol 2017;13:548–54.
[4] Birdno MJ, Grill WM. Mechanisms of deep brain stimulation in movement disorders as revealed by changes in stimulus frequency. Neurotherapeutics 2008;5:14–25.
[5] Lozano AM, Lipsman N, Bergman H, Brown P, Chabardes S, Chang JW, et al. Deep brain stimulation: current challenges and future directions. Nat Rev Neurol 2019;15:148–60.
[6] Bucher D, Goaillard JM. Beyond faithful conduction: short-term dynamics, neuromodulation, and long-term regulation of spike propagation in the axon. Prog Neurobiol 2011;94:307–46.
[7] García MR, Pearlmutter BA, Wellstead PE, Middleton RH. A slow axon antidromic blockade hypothesis for tremor reduction via deep brain stimulation. PLoS One 2013;8:e73456.
[8] Coenen VA, Allert N, Paus S, Kronenbürger M, Urbach H, Mädler B. Modulation of the cerebello-thalamo-cortical network in thalamic deep brain stimulation for tremor. Neurosurgery 2014;75:657–70.
[9] Gravbrot N, Saranathan M, Pouratian N, Kasoff WS. Advanced imaging and direct targeting of the motor thalamus and dentato-rubro-thalamic tract for tremor: a systematic review. Stereotact Funct Neurosurg 2020;98:220–40.
[10] Petersen KJ, Reid JA, Chakravorti S, Juttukonda MR, Franco G, Trujillo P, et al. Structural and functional connectivity of the nondecussating dentato-rubro-thalamic tract. Neuroimage 2018;176:364–71.
[11] Coenen VA, Allert N, Madler B. A role of diffusion tensor imaging fiber tracking in deep brain stimulation surgery: DBS of the dentato-rubro-thalamic tract (drt) for the treatment of therapy-refractory tremor. Acta Neurochir 2011;153:1579–85. discussion 1585.
[12] Ranck Jr JB. Which elements are excited in electrical stimulation of mammalian central nervous system: a review. Brain Res 1975;98:417–40.
[13] Fenoy AJ, Simpson Jr RK. Risks of common complications in deep brain stimulation surgery: management and avoidance. J Neurosurg 2014;120:132–9.
[14] Dale AM, Fischl B, Sereno MI. Cortical surface-based analysis. I. Segmentation and surface reconstruction. Neuroimage 1999;9:179–94.
[15] Fischl B, van der Kouwe A, Destrieux C, Halgren E, Ségonne F, Salat DH, et al. Automatically parcellating the human cerebral cortex. Cerebr Cortex 2004;14:11–22.
[16] Cox RW. AFNI: software for analysis and visualization of functional magnetic resonance neuroimages. Comput Biomed Res 1996;29:162–73.
[17] Conner CR, Ellmore TM, DiSano MA, Pieters TA, Potter AW, Tandon N. Anatomic and electro-physiologic connectivity of the language system: a combined DTI-CCEP study. Comput Biol Med 2011;41:1100–9.
[18] Chen W, de Hemptinne C, Miller AM, Leibbrand M, Little SJ, Lim DA, et al. Prefrontal-Subthalamic hyperdirect pathway modulates movement inhibition in humans. Neuron 2020;106:579–88.
[19] Gordon B, Lesser RP, Rance NE, Hart J jr, Webber R, Uematsu S, et al. Parameters for direct cortical electrical stimulation in the human: histopathologic confirmation. Electroencephalogr Clin Neurophysiol 1990;75:371–7.
[20] Merrill DR, Bikson M, Jefferys JG. Electrical stimulation of excitable tissue: design of efficacious and safe protocols. J Neurosci Methods 2005;141:171–98.
[21] Cogan SF, Ludwig KA, Welle CG, Takmakov P. Tissue damage thresholds during therapeutic electrical stimulation. J Neural Eng 2016;13:021001.
[22] Voytek B, D'Esposito M, Crone N, Knight RT. A method for event-related phase/amplitude coupling. Neuroimage 2013;64:416–24.
[23] Canolty RT, Edwards E, Dalal SS, Soltani M, Nagarajan SS, Kirsch HE, et al. High gamma power is phase-locked to theta oscillations in human neocortex. Science 2006;313:1626–8.
[24] Tort AB, Komorowski R, Eichenbaum H, Kopell N. Measuring phase-amplitude coupling between neuronal oscillations of different frequencies. J Neurophysiol 2010;104:1195–210.
[25] de Hemptinne C, Swann NC, Ostrem JL, Ryapolova-Webb ES, San Luciano M, Galifianakis NB, et al. Therapeutic deep brain stimulation reduces cortical phase-amplitude coupling in Parkinson's disease. Nat Neurosci 2015;18:779–86.
[26] Urbano FJ, Rosato-Siri MD, Uchitel OD. Calcium channels involved in neurotransmitter release at adult, neonatal and P/Q-type deficient neuromuscular junctions (Review). Mol Membr Biol 2002;19:293–300.
[27] Holsheimer J, Demeulemeester H, Nuttin B, de Sutter P. Identification of the target neuronal elements in electrical deep brain stimulation. Eur J Neurosci 2000;12:4573–7.
[28] Holsheimer J, Dijkstra EA, Demeulemeester H, Nuttin B. Chronaxie calculated from current-duration and voltage-duration data. J Neurosci Methods 2000;97:45–50.
[29] Kuncel AM, Grill WM. Selection of stimulus parameters for deep brain stimulation. Clin Neurophysiol 2004;115:2431–41.
[30] Grill WM, Mcintyre CC. Extracellular excitation of central neurons: implications for the mechanisms of deep brain stimulation. Thalamus Relat Syst 2001;1:269–77.
[31] Howell B, Isbaine F, Willie JT, Opri E, Gross RE, Hemptinne CD, et al. Image-based biophysical modeling predicts cortical potentials evoked with subthalamic deep brain stimulation. Brain Stimul 2021;14:549–63.
[32] Buzsáki G, Anastassiou CA, Koch C. The origin of extracellular fields and currents–EEG, ECoG, LFP and spikes. Nat Rev Neurosci 2012;13:407–20.
[33] Limousin P, Pollak P, Benazzouz A, Hoffmann D. Effect on parkinsonian signs and symptoms of bilateral subthalamic nucleus stimulation. Lancet 1995;345:91–5.
[34] Grill WM, Snyder AN, Miocinovic S. Deep brain stimulation creates an informational lesion of the stimulated nucleus. Neuroreport 2004;15:1137–40.
[35] Birdno MJ, Kuncel AM, Dorval AD, Turner DA, Gross RE, Grill WM. Stimulus features underlying reduced tremor suppression with temporally patterned deep brain stimulation. J Neurophysiol 2012;107:364–83.
[36] Eusebio A, Pogosyan A, Wang S, Averbeck B, Gaynor LD, Cantiniaux S, et al. Resonance in subthalamo-cortical circuits in Parkinson's disease. Brain 2009;132:2139–50.
[37] Baker KB, Montgomery EB, Rezai AR, Burgess R, Lüders HO. Subthalamic nucleus deep brain stimulus evoked potentials: physiological and therapeutic implications. Mov Disord 2002;17:969–83.
[38] Herrington TM, Cheng JJ, Eskandar EN. Mechanisms of deep brain stimulation. J Neurophysiol 2016;115:19–38.
[39] Miocinovic S, de Hemptinne C, Chen W, Isbaine F, Willie JT, Ostrem JL, et al. Cortical potentials evoked by subthalamic stimulation demonstrate a short latency hyperdirect pathway in humans. J Neurosci 2018;38:9129–41.
[40] Kent AR, Swan BD, Brocker DT, Turner DA, Gross RE, Grill WM. Measurement of evoked potentials during thalamic deep brain stimulation. Brain Stimul 2015;8:42–56.